Silicon nitride electric-field poled microresonator modulator

Boris Zabelich ; Christian Lafforgue ; Edgars Nitiss ; Anton Stroganov ; Camille-Sophie Brès ✉

Check for updates

CrossMark

View Online

Export Citation

Silicon nitride electric-field poled microresonator modulator

View Online   Export Citation   CrossMark

Boris Zabelich,[1] (ID) Christian Lafforgue,[1] (ID) Edgars Nitiss,[1] (ID) Anton Stroganov,[2] (ID)
and Camille-Sophie Brès[1,a)] (ID)

AFFILIATIONS

[1] Ecole Polytechnique Fédérale de Lausanne, Photonic Systems Laboratory (PHOSL), CH-1015 Lausanne, Switzerland
[2] LIGENTEC SA, EPFL Innovation Park, CH-1024 Ecublens, Switzerland

[a)]Author to whom correspondence should be addressed: camille.bres@epfl.ch

ABSTRACT

Stoichiometric silicon nitride is a highly regarded platform for its favorable attributes, such as low propagation loss and compatibility with complementary metal-oxide-semiconductor technology, making it a prominent choice for various linear and nonlinear applications on a chip. However, due to its amorphous structure, silicon nitride lacks second-order nonlinearity; hence, the platform misses the key functionality of linear electro-optical modulation for photonic integrated circuits. Several approaches have been explored to address this problem, including integration with electro-optic active materials, piezoelectric tuning, and utilization of the thermo-optic effect. In this work, we demonstrate electro-optical modulation in a silicon nitride microring resonator enabled by electric-field poling, eliminating the complexities associated with material integration and providing data modulation speeds up to 75 Mb/s, currently only limited by the electrode design. With an estimated inscribed electric field of 100 V/μm, we achieve an effective second-order susceptibility of 0.45 pm/V. In addition, we derive and confirm the value of the material's third-order susceptibility, which is responsible for the emergence of second-order nonlinearity. These findings broaden the functionality of silicon nitride as a platform for electro-optic modulation.

I. INTRODUCTION

The amorphous structure of the low-loss stoichiometric silicon nitride (Si_3N_4) platform presents a challenge in harnessing the linear electro-optical effect.[1] However, unlocking the potential for phase and amplitude modulation in this CMOS-compatible material would significantly expand its range of applications. In order to enable refractive index tuning in Si_3N_4 waveguide structures for applications such as optical frequency comb control,[2–4] laser stabilization,[5,6] and data modulation,[7–9] several methods have been explored. These methods include the utilization of the thermo-optic effect, piezoelectric actuation, and integration with materials having intrinsic second-order ($\chi^{(2)}$) nonlinearity. Despite their potential, these methods suffer from certain drawbacks. Thermal heating leads to excessive power consumption, while the modulation speed is limited to several tens of kHz. Integrating electro-optic active or piezoelectric materials with Si_3N_4 introduces complexities in the fabrication process and may result in higher optical

losses. Consequently, researchers are actively investigating other routes to enable $\chi^{(2)}$ nonlinear processes within Si_3N_4,[10–12] aiming to overcome these limitations.

One alternative approach to induce second-order nonlinearity exclusively within Si_3N_4 involves symmetry breaking through the permanent charge relocation and the inscription of an electric field (E_{ins}) within the material. This process gives rise to an effective second-order susceptibility ($\chi_{eff}^{(2)}$), which arises from the coupling between the inscribed electric field and the material's third-order susceptibility ($\chi^{(3)}$), expressed by the relation $\chi_{eff}^{(2)} = 3\chi^{(3)}E_{ins}$. All-optical poling (AOP)[13–15] and electric-field poling[11,16] are two techniques that can be utilized to move the electric charges within the material to establish a permanent electric field.

In AOP, the absorption interference of three coherent waves satisfying energy conservation described by the coherent photogalvanic effect[17] is responsible for the asymmetric charge ionization and inscription of a space-charge grating along the waveguide,

inducing $\chi_{\text{eff}}^{(2)}$. Leveraging this effect, several applications have been demonstrated in various Si$_3$N$_4$ structures, including sum and difference frequency generation[18–20] and the generation of quantum states of light,[21] to name a few. On the other hand, the thermally assisted electric-field poling technique[16] exploits the movement of thermally activated charges within the material under the influence of an externally applied electric field. The charge relocation results in the inscription of a uniform electric field along the waveguide, enabling linear electro-optical (LEO) modulation. After the poling process, the device can effectively function as a linear electro-optical modulator, particularly for modulation fields significantly smaller than the inscribed electric field.

In this work, we demonstrate an integrated electro-optic modulator based solely on Si$_3$N$_4$, capable of achieving data modulation speeds of up to 75 Mb/s, currently limited by the electrode design. Through thermally assisted electric field poling, a uniform electric field is inscribed within the Si$_3$N$_4$ microring, enabling linear electro-optical modulation. This approach alleviates the need for complex co-integration of materials for the linear electro-optic modulation, providing a modulation speed much higher than the thermo-optic effect without affecting the optical losses of the waveguide. With an inscribed field magnitude of 100 V/μm, we achieve a $\chi_{\text{eff}}^{(2)}$ of 0.45 pm/V. In the context of a growing Si$_3$N$_4$ photonic platform, this demonstration is a step forward toward high-functionality photonic integrated circuits, currently lacking low-cost, high-speed EO modulators.

II. DEVICE DESIGN AND OPTICAL CHARACTERIZATION

Figures 1(a) and 1(b) show the schematic top view of the device and its cross section. The device fabricated by LIGENTEC using its AN800 technology platform consists of a Si$_3$N$_4$ microring and a bus waveguide, an aluminum electrode on top of the microring, and a conductive silicon substrate (10–25 Ω cm). The microring radius is 476.8 μm, corresponding approximately to the 50 GHz free-spectral range in the C-band, and has a cross section of 1 ×0.8 μm^2. The bus waveguide with a cross section of 0.84 ×0.8 μm^2 is placed 0.3 μm away from the microring for efficient coupling of both light polarizations. The Si$_3$N$_4$ structures are buried in silica 4 μm above the substrate. The signal electrode has a width of 10 μm and is located 1.7 μm above the waveguide, covering 90% of the ring circumference.
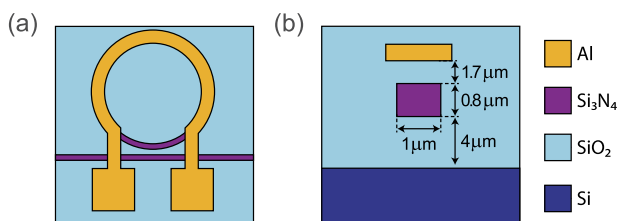

FIG. 1. (a) and (b) Schematic top view and the cross section of the device under study. Dimensions are not to scale. The device comprises a Si$_3$N$_4$ waveguide core buried in SiO$_2$ cladding, a conductive Si substrate, and an aluminum (Al) electrode above the waveguide covering 90% of the microring circumference.
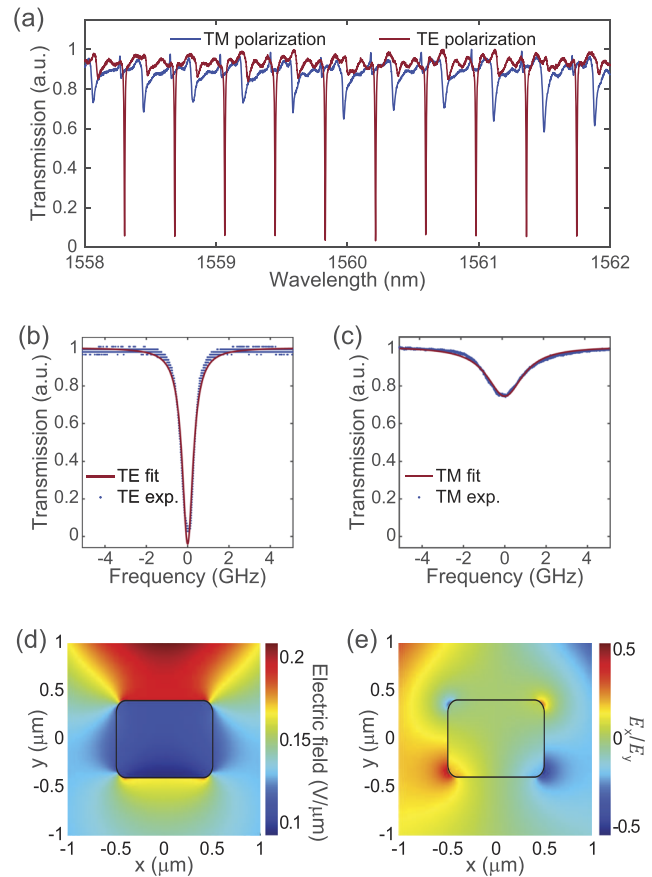

FIG. 2. (a) Measured transmission spectra of the microring resonator with TE (red) and TM (blue) polarized light. (b) and (c) Quality factor (Q factor) measurements of the resonances used in the study for TE and TM polarized light at 1560.60 and 1560.75 nm, respectively. (d) Simulated electric field profile at 1 V applied. (e) The ratio of horizontal and vertical components of the applied electric field (E_x/E_y) in the waveguiding area.

We characterized the optical resonances of the device using a tunable mode-hop-free source in the C-band range (Toptica CTL 1550). The optical transmission spectra in Fig. 2(a) reveal single-mode operation with critically coupled and slightly undercoupled regimes for TE and TM polarized light, respectively. Figures 2(b) and 2(c) show the resonances near 1560 nm for TE and TM polarized light, respectively, used for the subsequent electro-optic characterization of the device. To acquire a precise measurement of the quality factor of the studied resonances, the laser frequency is tuned across the resonances with a built-in piezo driver. The change in frequency during the scan is calibrated using the sideband modulation technique.[22] The measured resonance widths for TE and TM polarized light are 0.64 and 2.2 GHz, respectively, corresponding to the loaded Q factors of 3.0×10^5 and 0.9×10^5.

Using a finite element solver (COMSOL Multiphysics), the optical modes and the externally applied electric field profiles were simulated. In this study, the aluminum electrode initially designed

09 February 2024 14:44:19

for thermal heating was used as a signal electrode, while the conductive substrate served as a ground electrode. The amplitude of the simulated electric field reaches 0.1 V/μm in the center of the waveguide for 1 V applied, as shown in Fig. 2(d). Due to the relative position of the electrodes, the electric field is aligned predominantly vertically, as indicated by the ratio of the horizontal and vertical components of the applied electric field (E_x/E_y) plotted in Fig. 2(e). This allows us to independently consider two tensor elements of the third-order susceptibility responsible for the quadratic electro-optic effect with TE and TM polarized light. For the collinear relative polarization of the optical and externally applied electric fields, the relevant third-order susceptibility tensor element is $\chi^{(3)}_{1111}$ (TM mode case), while for the orthogonal relative polarization, it is $\chi^{(3)}_{1122}$ (TE mode case).

III. QUADRATIC ELECTRO-OPTIC EFFECT

Prior to electric-field poling and characterization of the linear electro-optic modulation of the device, we studied the resonance shift due to the quadratic electro-optic effect under an externally applied electric field to extract the values of the third-order susceptibility tensor elements related to the DC Kerr effect. For this purpose, the setup schematically drawn in Fig. 3(a) was used. Linearly polarized light from the tunable laser goes through a polarization controller and is coupled to the device with a lensed

(a)

(b)

FIG. 3. (a) Experimental set-up for the measurement of the quadratic electro-optic effect. PC: polarization controller, Obj.: objective, PD: photodetector, and HV source: high voltage source. (b) The resonance shift for TE (in red) and TM (in blue) polarized light as a function of the applied voltage before electric-field poling.

fiber. The outcoupled light is collected using a microscope objective and then delivered to a fast photodetector (New Focus 1811). The ground electrode of a high-voltage source (LabSmith HVS448 6000D) is connected to the conductive silicon substrate while the voltage is applied to the signal electrode on top of the microresonator. A resonance shift is detected under the applied voltage by sweeping the laser frequency while the light transmission is recorded.

Figure 3(b) shows the measured resonance shifts vs applied voltage for TE (in red) and TM (in blue) polarized light. The change in the resonance position has the characteristic parabolic dependence of the DC Kerr effect on the applied voltage centered at 0 V, indicating the absence of any significant intrinsic $\chi^{(2)}$ in the material. The resonance shift reaches 0.6 and 1 GHz at 1000 V (100 V/μm in the center of the waveguide core) applied for TE and TM polarized light, respectively. The change in the effective refractive index Δn_{eff} can be related to the resonance shift $\Delta\nu$ using the equation below

$$\frac{\Delta\nu}{\nu_{\text{res}}} = \frac{L_{\text{elec}}}{L_{\text{ring}}}\frac{\Delta n_{\text{eff}}}{n_g}, \tag{1}$$

where ν_{res} is the resonance frequency, n_g is the group index of the waveguide, and L_{ring} and L_{elec} are the ring perimeter and electrode length, respectively. From the experimental values of the resonance shift and the simulated group index, the change in the effective refractive index can be calculated for a particular mode. The calculated maximum Δn_{eff} for TE and TM polarized light are 7.6×10^{-6} and 1.3×10^{-5}, respectively. With the known value of the effective refractive index change, the values of the relevant $\chi^{(3)}$ tensor elements can be calculated considering the overlap between the optical (E_{opt}) and the electric (E_{el}) fields within the waveguiding medium.[16,23,24] Calculating the overlap integral, we found the relevant values of $\chi^{(3)}$ tensor elements to be $\chi^{(3)}_{1122} = (0.88 \pm 0.03) \times 10^{-21}$ m^2/V^2 and $\chi^{(3)}_{1111} = (1.46 \pm 0.07) \times 10^{-21}$ m^2/V^2, which are in excellent agreement with the previously obtained values.[16] These values are used to estimate the induced $\chi^{(2)}_{\text{eff}}$ and the profile of the inscribed electric field.

IV. INDUCED SECOND-ORDER NONLINEARITY

After the initial characterization of the device, $\chi^{(2)}_{\text{eff}}$ was induced within the Si$_3$N$_4$ microring via thermally-assisted electric-field poling. In this process, the chip was placed onto a hot ceramic plate at 260 °C, consistent with our previous study,[16] and then a high voltage of 1000 V was applied for 1 hour. During this period of time, the thermally activated charges within Si$_3$N$_4$ moved under the externally applied field. Afterward, the heating was turned off while the poling field was maintained until the system cooled down to room temperature, fixing the position of the driven charges within the material. This charge relocation resulted in the formation of a static electric field within the Si$_3$N$_4$ microring, inducing an effective second-order nonlinearity.

The device was poled with the poling voltage $V_p = 1000$ V (100 V/μm in the center of the waveguide), and Fig. 4(a) shows the subsequently measured resonance shifts with the applied DC voltage for TE and TM polarized light. In the new state of the device,
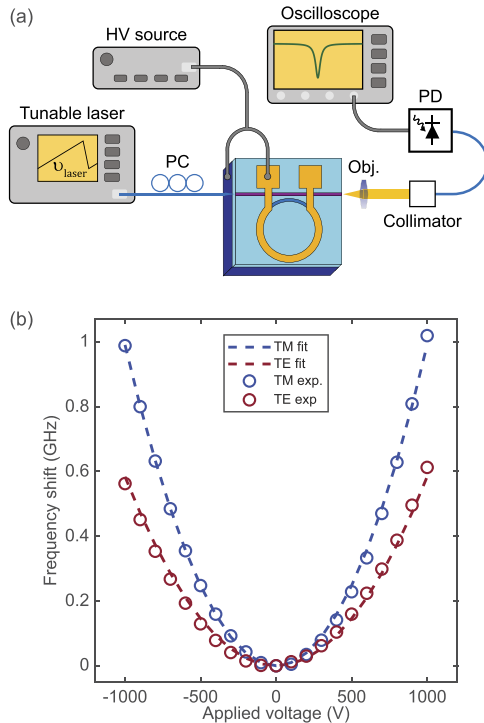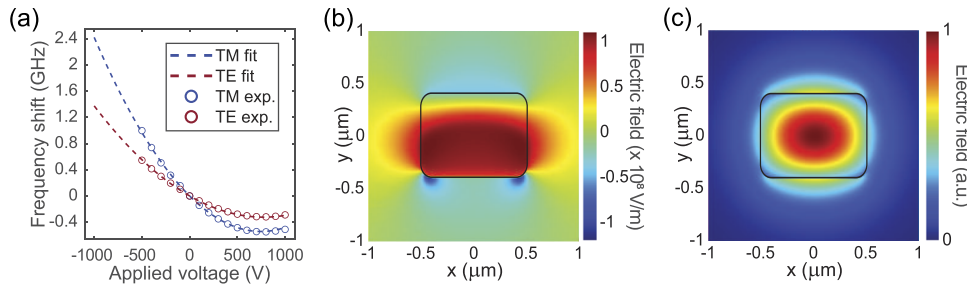
FIG. 4. (a) Resonance shift for TE (in red) and TM (in blue) polarized light as a function of the applied voltage after electric-field poling with V_p = 1000 V. (b) The simulated inscribed electric field distribution after electric-field poling for V_p = 1000 V. (c) Simulated TM mode profile inside the microring waveguide.

both the linear and quadratic electro-optic effects contribute to the refractive index change, as shown in the following equation:

$$\Delta n = \frac{3}{2}\frac{\chi^{(3)}E_0^2}{n_0} + \frac{3\chi^{(3)}E_0 E_{ins}}{n_0} = \frac{3}{2}\frac{\chi^{(3)}E_0^2}{n_0} + \frac{\chi_{eff}^{(2)}E_0}{n_0}, \quad (2)$$

where E_0 is the applied electric field. After electric-field poling, the frequency shift has the form of a parabola displaced relative to 0 V. The shift of the parabola vertices to the positive value of the applied voltage indicates the inscription of the electric field in the opposite direction.

In the case of small applied voltages, the electro-optic response can be approximated by a linear function as the inscribed field is much higher than the applied signal [the second term in Eq. (2)]. For instance, for the device poled with V_p = 1000 V, when fitting the experimental data for TM polarized light with a second-order polynomial ($y = ax^2 + bx + c$) and assuming an applied voltage of 5 V, the ratio $b/(a \cdot 5$ V$)$ is found to be ~300. This observation highlights the dominant contribution of the linear electro-optic effect to the Δn_{eff} with small applied voltages. The calculated frequency shifts per 1 V applied are 0.8 and 1.4 MHz/V for TE and TM polarized light, respectively. The quadratic terms remained the same after the poling procedure, indicating no change in the values of the relevant $\chi^{(3)}$ tensor elements. It is important to note that electric-field poling did not affect the optical losses of the waveguide, as evidenced by the identical values of the measured loaded Q factors of the resonances under study.

The parabola vertices for both light polarizations are located at around 770 V, a value that does not match the poling voltage of 1000 V. As explained in more detail below, due to the origin of the inscribed electric field connected to the movement of the thermally activated charges, the profiles of the inscribed and externally applied electric fields differ. It results in a diminished value of the overlap integral of the interacting fields; therefore, a lower value of the applied voltage is required to balance the linear and quadratic electro-optic effects in the poled device.

To provide an explanation for the observed changes in the electro-optical response after the electric-field poling process, we utilized a two-dimensional model developed in our previous work.[16] This model accounts for the redistribution of charges within Si_3N_4 under an applied electric field, resulting in the formation of a built-in electric field. Our model is based on the simulations in the study by Camara *et al.*[25] describing the ion-exchange process during the

thermal poling of silica fibers. In our model, we assume the electrical neutrality of the Si_3N_4 waveguide cross section, which is defined by an even distribution of negatively and positively charged particles. In our previous work, we found that hydrogen ions can be the species responsible for the electric field inscription; hence, the sign of the mobile charges was chosen to be positive. The movement of the charges is confined to the bounds of the waveguide, preventing charge leakage. For the numerical simulations, the diffusion coefficient is set to be 1×10^{-18} m²/s within the bounds defined in our previous study, ensuring a steady state of the system after 1 h of poling. By varying the available charge concentration within the Si_3N_4 waveguide, we simulated the magnitude and profile of the electric field, which were later used to calculate the induced refractive index change under externally applied voltage and to fit the experimental data.

Using the described methodology, the charge concentration was derived to be $C = 0.33 \pm 0.05$ mol/m³. The simulated inscribed electric field profile is shifted to the bottom of the waveguide [Fig. 4(b)] as cations were forced to move from the source of the externally applied field, forming a depleted zone. As a result, the overlap of an optical mode [for instance, the TM mode depicted in Fig. 4(c)] with the inscribed electric field is less optimal than with the externally applied field, explaining the value mismatch between V_p and the parabola vertex positions. The magnitude of the inscribed field in the center of the waveguide is 100 V/μm, resulting in the largest induced $\chi_{eff}^{(2)}$ of 0.45 pm/V.

It is important to emphasize that the same device can undergo multiple cycles of the electric field inscription process without any change in the induced second-order nonlinearity. Complete charge relaxation is achieved by exposing the chip to a temperature of 300 °C for a continuous 24-h period. Following the heating process, the resonance shift as a function of the applied voltage exhibits the same parabolic form centered at 0 V, similar to what is illustrated in Fig. 3(b). Subsequent electric field inscription, under the same poling conditions (poling voltage of 1000 V at 260 °C), results in the same induced second-order nonlinearity as observed after the initial poling process.

We also noted that the induced second-order nonlinearity slowly decays in time at room temperature. By monitoring the resonance shift with the applied DC voltage in time and assessing a change in the fitting coefficient responsible for the linear electro-optic effect, we found a 35% reduction in the observed $\chi_{eff}^{(2)}$ within
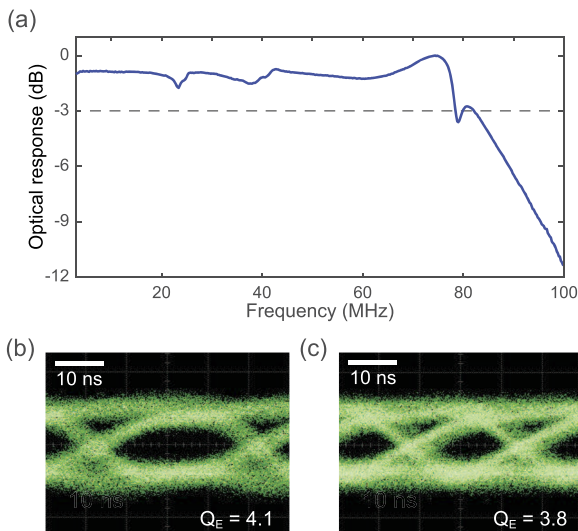
09 February 2024 14:44:19

FIG. 5. (a) Optical response as a function of the RF frequency showing a 3-dB bandwidth of 78 MHz for the device under study. (b) and (c) Eye diagrams at 50 and 75 Mb/s measured with a non-return-to-zero scheme (2^{31}-1 pseudorandom binary sequence) and a peak-to-peak drive voltage V_{pp} = 10 V.

54 days. For longer periods, we expect a decrease in the relaxation speed similar to the observed decay of the induced second-order nonlinearity in all-optically poled Si_3N_4 waveguides.[15]

V. ELECTRO-OPTIC MODULATION

After electric-field poling, the frequency response of the Si_3N_4 microring modulator was measured using a vector network analyzer (Anritsu MS2036C) and a 125 MHz bandwidth photodetector (New Focus 1811). As shown in Fig. 5(a), the 3-dB modulation bandwidth of the device under study is 78 MHz. We believe that the maximal operation bandwidth is limited by the high capacitance of the electrode design as well as the high resistance of the probe contacts. The calculated cavity photon lifetime of 230 ps corresponds to a modulation bandwidth of around 640 MHz.

The data rate operation of our device was tested using a 2^{31}-1 non-return-to-zero pseudorandom binary sequence from a high-speed pattern generator (Anritsu MP1763C). With the modulating peak-to-peak voltage V_{pp} of 10 V, the open eye diagrams at 50 and 75 Mb/s bitrates were observed with the eye Q-factors Q_E of 4.1 and 3.8, respectively, as demonstrated in Figs. 5(b) and 5(c).

VI. DISCUSSION AND CONCLUSIONS

In this study, we have demonstrated the functionality of a Si_3N_4 microresonator as an electro-optical modulator enabled by electric-field poling. The use of Si_3N_4 as an active electro-optic material mitigates the need for complex co-integration with materials possessing an intrinsic second-order nonlinearity to enable linear electro-optical modulation. For the poling voltage of 1000 V, we achieved an inscribed electric field strength of 100 V/μm in the center of the waveguide, providing an effective second-order susceptibility of 0.45 pm/V. The proof-of-principle modulator exhibited a bandwidth of 78 MHz, limited by the electrode design, while the photon lifetime of the resonance under interest indicated the potential for modulation frequencies of several hundreds of MHz. To evaluate the data transmission capabilities, we conducted experiments using a modulation peak-to-peak voltage of 10 V and obtained open eye diagrams for bitrates of 50 and 75 Mb/s.

This study further confirms the potential of Si_3N_4 as a platform for electro-optical modulation while maintaining low propagation loss. To enhance the device's performance, several approaches can be explored. First, higher poling electric field strengths can be considered to induce greater second-order nonlinearity within Si_3N_4. With the reported value of Si_3N_4 electrical breakdown strength of 300 V/μm,[26] it is potentially possible to achieve $\chi_{\text{eff}}^{(2)}$ values up to 1.3 pm/V. Second, silicon-rich silicon nitride is another silicon-based amorphous material providing a higher $\chi^{(3)}$ value that could be a promising candidate for electric-field poling, enabling higher induced second-order nonlinearity.[27] A recent study[28] demonstrated the material's suitability for all-optical poling, validating its charge relocation capability for electric field inscription. Finally, to make the effect of electric-field poling long-lasting, optical activation of charges could be explored, as it was done in silica fibers.[29] With the illumination of the material with an optical source of high-energy photons, the deeper trap states could be excited, releasing the charges for the electric field inscription. The reported results on electro-optical modulation in Si_3N_4 pave the way for new applications in integrated photonics based on this low-loss, CMOS-compatible platform.

AUTHOR DECLARATIONS

Conflict of Interest

The authors have no conflicts to disclose.

Author Contributions

Boris Zabelich: Conceptualization (equal); Data curation (equal); Formal analysis (equal); Writing – original draft (equal). **Christian Lafforgue**: Formal analysis (equal); Investigation (equal); Writing – original draft (equal). **Edgars Nitiss**: Formal analysis (equal); Investigation (equal). **Anton Stroganov**: Resources (equal). **Camille-Sophie Brès**: Funding acquisition (equal); Project administration (equal); Supervision (equal); Writing – review & editing (equal).

DATA AVAILABILITY

The data that support the findings of this study are available from the corresponding author upon reasonable request.

09 February 2024 14:44:19

REFERENCES

[1] R. W. Boyd, *Nonlinear Optics* (Academic Press, 2008).

[2] X. Xue, Y. Xuan, C. Wang, P.-H. Wang, Y. Liu, B. Niu, D. E. Leaird, M. Qi, and A. M. Weiner, "Thermal tuning of Kerr frequency combs in silicon nitride microring resonators," Opt. Express **24**, 687–698 (2016).

[3] C. Joshi, J. K. Jang, K. Luke, X. Ji, S. A. Miller, A. Klenner, Y. Okawachi, M. Lipson, and A. L. Gaeta, "Thermally controlled comb generation and soliton modelocking in microresonators," Opt. Lett. **41**, 2565–2568 (2016).

[4] S. A. Miller, Y. Okawachi, S. Ramelow, K. Luke, A. Dutt, A. Farsi, A. L. Gaeta, and M. Lipson, "Tunable frequency combs based on dual microring resonators," Opt. Express **23**, 21527–21540 (2015).

[5] J. Wang, K. Liu, M. W. Harrington, R. Q. Rudy, and D. J. Blumenthal, "Silicon nitride stress-optic microresonator modulator for optical control applications," Opt. Express **30**, 31816–31827 (2022).

[6] G. Lihachev, J. Riemensberger, W. Weng, J. Liu, H. Tian, A. Siddharth, V. Snigirev, V. Shadymov, A. Voloshin, R. N. Wang, J. He, S. A. Bhave, and T. J. Kippenberg, "Low-noise frequency-agile photonic integrated lasers for coherent ranging," Nat. Commun. **13**, 3522 (2022).

[7] K. Alexander, J. P. George, J. Verbist, K. Neyts, B. Kuyken, D. Van Thourhout, and J. Beeckman, "Nanophotonic Pockels modulators on a silicon nitride platform," Nat. Commun. **9**, 3444 (2018).

[8] P. Zhang, H. Huang, Y. Jiang, X. Han, H. Xiao, A. Frigg, T. G. Nguyen, A. Boes, G. Ren, Y. Su, Y. Tian, and A. Mitchell, "High-speed electro-optic modulator based on silicon nitride loaded lithium niobate on an insulator platform," Opt. Lett. **46**, 5986–5989 (2021).

[9] N. Boynton, H. Cai, M. Gehl, S. Arterburn, C. Dallo, A. Pomerene, A. Starbuck, D. Hood, D. C. Trotter, T. Friedmann, C. T. DeRose, and A. Lentine, "A heterogeneously integrated silicon photonic/lithium niobate travelling wave electro-optic modulator," Opt. Express **28**, 1868–1884 (2020).

[10] C. Castellan, A. Trenti, C. Vecchi, A. Marchesini, M. Mancinelli, M. Ghulinyan, G. Pucker, and L. Pavesi, "On the origin of second harmonic generation in silicon waveguides with silicon nitride cladding," Sci. Rep. **9**, 1088 (2019).

[11] Y. Zhang, J. Nauriyal, M. Song, M. Granados Baez, X. He, T. Macdonald, and J. Cardenas, "Engineered second-order nonlinearity in silicon nitride," Opt. Mater. Express **13**, 237–246 (2023).

[12] S. Miller, Y.-H. D. Lee, J. Cardenas, A. L. Gaeta, and M. Lipson, "Electro-optic effect in silicon nitride," in *CLEO: Science and Innovations* (Optica Publishing Group, 2015), p. SF1G–4.

[13] D. D. Hickstein, D. R. Carlson, H. Mundoor, J. B. Khurgin, K. Srinivasan, D. Westly, A. Kowligy, I. I. Smalyukh, S. A. Diddams, and S. B. Papp, "Self-organized nonlinear gratings for ultrafast nanophotonics," Nat. Photonics **13**, 494–499 (2019).

[14] A. Billat, D. Grassani, M. H. Pfeiffer, S. Kharitonov, T. J. Kippenberg, and C.-S. Brès, "Large second harmonic generation enhancement in Si_3N_4 waveguides by all-optically induced quasi-phase-matching," Nat. Commun. **8**, 1016 (2017).

[15] E. Nitiss, T. Liu, D. Grassani, M. Pfeiffer, T. J. Kippenberg, and C.-S. Brès, "Formation rules and dynamics of photoinduced $\chi^{(2)}$ gratings in silicon nitride waveguides," ACS Photonics **7**, 147–153 (2019).

[16] B. Zabelich, E. Nitiss, A. Stroganov, and C.-S. Brès, "Linear electro-optic effect in silicon nitride waveguides enabled by electric-field poling," ACS Photonics **9**, 3374–3383 (2022).

[17] O. Yakar, E. Nitiss, J. Hu, and C.-S. Brès, "Generalized coherent photogalvanic effect in coherently seeded waveguides," Laser Photonics Rev. **16**, 2200294 (2022).

[18] J. Hu, E. Nitiss, J. He, J. Liu, O. Yakar, W. Weng, T. J. Kippenberg, and C.-S. Brès, "Photo-induced cascaded harmonic and comb generation in silicon nitride microresonators," Sci. Adv. **8**, eadd8252 (2022).

[19] D. Grassani, M. H. Pfeiffer, T. J. Kippenberg, and C.-S. Brès, "Second- and third-order nonlinear wavelength conversion in an all-optically poled Si_3N_4 waveguide," Opt. Lett. **44**, 106–109 (2019).

[20] E. Sahin, B. Zabelich, O. Yakar, E. Nitiss, J. Liu, R. N. Wang, T. J. Kippenberg, and C.-S. Brès, "Difference-frequency generation in optically poled silicon nitride waveguides," Nanophotonics **10**, 1923–1930 (2021).

[21] R. Dalidet, F. Mazeas, E. Nitiss, O. Yakar, A. Stroganov, S. Tanzilli, L. Labonté, and C.-S. Brès, "Near perfect two-photon interference out of a down-converter on a silicon photonic chip," Opt. Express **30**, 11298–11305 (2022).

[22] J. Li, H. Lee, K. Y. Yang, and K. J. Vahala, "Sideband spectroscopy and dispersion measurement in microcavities," Opt. Express **20**, 26337–26344 (2012).

[23] J. Peltier, W. Zhang, L. Virot, C. Lafforgue, L. Deniel, D. Marris-Morini, G. Aubin, F. Amar, D. Tran, X. Yan, C. G. Littlejohns, C. Alonso-Ramos, D. J. Thomson, G. Reed, and L. Vivien, "High speed silicon photonic electro-optic Kerr modulation," arXiv:2302.13768 (2023).

[24] A. Honardoost, R. Safian, A. Rao, and S. Fathpour, "High-speed modeling of ultracompact electrooptic modulators," J. Lightwave Technol. **36**, 5893–5902 (2018).

[25] A. Camara, O. Tarasenko, and W. Margulis, "Study of thermally poled fibers with a two-dimensional model," Opt. Express **22**, 17700–17715 (2014).

[26] C. Rauthan and J. Srivastava, "Electrical breakdown voltage characteristics of buried silicon nitride layers and their correlation to defects in the nitride layer," Mater. Lett. **9**, 252–258 (1990).

[27] D. Tan, K. Ooi, and D. Ng, "Nonlinear optics on silicon-rich nitride—A high nonlinear figure of merit CMOS platform [invited]," Photonics Res. **6**, B50–B66 (2018).

[28] O. Yakar, C. Lafforgue, A. Ayan, J. Faugier-Tovar, P. Chausse, C. Petit-Etienne, E. Pargon, Q. Wilmart, and C.-S. Brès, "Mid-IR all-optical poling in silicon nitride waveguides," in *CLEO: Science and Innovations* (Optica Publishing Group, 2023).

[29] J. M. Pereira, A. R. Camara, F. Laurell, O. Tarasenko, and W. Margulis, "Linear electro-optical effect in silica fibers poled with ultraviolet lamp," Opt. Express **27**, 14893–14902 (2019).